3803

SCANNING PROCESSING SHEEET

PROPERTY STAMP _____

COPYRIGHTED

YES (GREEN DOT) _____ NO ✓

DISPOSITION

	SCANNED COPY	COPY 2+
HIGH USE (RED DOT)	_____	_____
ARCHIVE (YELLOW DOT)	✓	_____
DISCARD (BLUE DOT)	_____	_____

CLASSIFICATION

U2 ✓ UL_____ CLASSIFIED_____

RESTRICTION STATEMENT

YES _____ NO ✓

SEARCH

DTIC ACCESSION NUMBER: _____
(ATTACH COPY OF STINET OR DROLS RECORD)

PUBLICATION DATE > 1/1/95

YES _____ NO _____

ELECTRONIC FULL TEXT AVAILABLE

STINET_____

DROLS _____

INTERNET _____

SCANNING

DTIC _____ TIC _____ Internet _____

BASIS/ACCESS CORRECTIONS REQUIRED

YES _____ NO _____

NUMBER OF IMAGES TO SCAN _____

File Name:C:\Mydocuments\ScanProc.doc
Revised 1/28/98

Accession Number: 3803

Publication Date: Aug 01, 1984

Title: Transverse Oscillation of Coaxial Multiple Beams Propagating Along a Magnetic Field in a Vacuum Tube

Personal Author: Chen, H.C.

Corporate Author Or Publisher: Naval Surface Weapons Center, White Oak Laboratory, Silver Spring, MD Report Number: NSWC MP 84-350 Report Number Assigned by Contract Monitor: 84-9

Comments on Document: Archive, RRI, DEW

Descriptors, Keywords: Directed Energy Weapon DEW Transverse Oscillation Coaxial Multiple Beam Propagation Magnetic Field Vacuum Tube Physics Theory Maxwell Theory Equation Drift Stability Analysis Perturbation Dispersion Relat

Pages: 34

Cataloged Date: Oct 19, 1992

Document Type: HC

Number of Copies In Library: 000001

Record ID: 24975

Source of Document: DEW

THE TRANSVERSE OSCILLATION OF COAXIAL MULTIPLE BEAMS PROPAGATING ALONG A MAGNETIC FIELD IN A VACUUM TUBE

H. C. CHEN

NSWC MP 84-350

PLASMA PHYSICS PUBLICATION NO. 84-9

AUGUST 1984

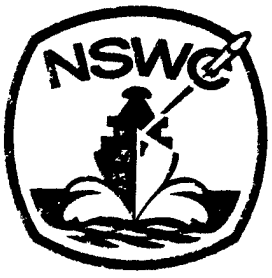

NAVAL SURFACE WEAPONS CENTER

SEP 09 1985

White Oak, Silver Spring, Maryland 20910

THE TRANSVERSE OSCILLATION OF COAXIAL MULTIPLE BEAMS PROPAGATING ALONG A MAGNETIC FIELD IN A VACUUM TUBE

H. C. CHEN
NAVAL SURFACE WEAPONS CENTER
WHITE OAK, SILVER SPRING, MARYLAND 20910

A fluid-Maxwell theory has been derived to study a system of multi-beams propagating parallel to an applied axial magnetic field in an evacuated conducting drift tube. The stability analysis is performed for a rigid-rotor and cold laminar flow equilibria. It is assumed that the particle beams are tenuous and the guiding field is very strong. As a result, the perturbation theory is derived under the condition that the plasma frequency is much smaller than the cyclotron frequency for each beam particle. A dispersion relation is obtained for a special case of sharp boundary density profiles. The stability properties of infinitely long beams are illustrated in detail for different geometries and various beam parameters. The results agree with those obtained by Uhm in a special case where a solid electron beam propagates through an annular electron beam. The finite geometry effect of the accelerator is discussed briefly. It might have a substantial influence on the behavior of a real device.

I. Introduction

There has been some resurgence of interest in the production of high-energy particle beams, especially ion beams, by the collective-acceleration process in the last few years. The collective particle accelerators, in principle, are designed to generate high-power particle beams by means of energy transfer from a negative-energy wave train grown on the intense annular relativistic electron beam. Generally, the electron beam propagates along a guided magnetic field inside an evacuated conducting drift tube [1]-[3]. The phase velocity of these travelling waves can be controlled by manipulating the beam parameters so that the particles to be accelerated can be trapped by the waves. As the wave energy increases, the trapped particles will be dragged and gain energy from the waves. However, there exist in practice some difficulties which stir numerous theoretical and experimental investigations. Naturally, the stability of this multi-beam system becomes one of the important subjects and big concerns in the acceleration process. The collective particle accelerator at NRL has suggested that a density modulated intense relativistic electron beam propagating in a spatially modulated magnetic field can drag particles and accelerate them to high energies. To make the problem tractable we simplify it by neglecting the beam modulation and rippled magnetic field and concentrate on the stability analysis of a two-beam system. The diocotron instability of a hollow coaxial multi-ring electron beam has been studied previously [4]-[6] using the fluid-Maxwell model for a broad range of beam parameters and different geometries. The same technique for stability analysis has been extended in this paper to investigate the most serious transverse oscillation for the general case of two different particle beams propagating along an external magnetic field. Nevertheless, the previously assumed infinitely long wavelength perturbation ($k = 0$) has been

removed. Furthermore, two beams are allowed not only to carry different charge and current, but also to travel in any direction with different speed along the tube.

A macroscopic cold fluid-Maxwell theory is used to perform the linear stability analysis of these infinitely long intense relativistic particle beams. Equilibrium properties of the beams along with the basic theory and assumptions are examined in Section II. In the linear regime, a set of eigenvalue equations for the perturbed field is derived in the rigid-rotor and cold laminar flow limit. In a special case where the density profile has sharp boundary, the magnetic field is strong and the particle beams are tenuous, a dispersion relation is derived in Section III and served as a tool to investigate the instability for a broad range of system parameters of experimental interest. In Section IV, the dispersion relation is solved numerically for various beam parameters. The stability properties are illustrated in great detail with particular emphasis on the beam current, beam location, beam charge and the velocities of the beam particles. Finally, we conclude the results of the instability which is based on the assumption of infinite long beams in Section V, with a brief discussion including the effect of finite geometry of the accelerator.

II. Basic theory and equilibrium state

The mechanism of a collective accelerator can accelerate ions as well as electrons. For the purpose of generality, let us consider the equilibrium configuration as illustrated in Figure 1. It consists of two cylindrically symmetric intense relativistic annular particle beams which propagate parallel to a uniform applied axial magnetic field $\underline{B}_0$ in vacuum through a smooth perfectly conducting drift tube of radius R_c. The cylindrical polar coordinates (r, θ, z) are used with the z-axis along the axis of symmetry. Two particle beams are located separately in between $R_1 < r < R_2$ and $R_3 < r < R_4$ respectively, and are characterized by their charge q_i, mass m_i, axial velocity $V_{zi} \equiv \beta_i c$ and density profile n_i. Where $i = 1$ and 2 represent the inner and outer beam respectively, c is the speed of light in vacuum. Normally, we allow partial neutralization by a small fraction of charges of opposite sign trapped in the beam. The influence of ion background on the stability of a relativistic electron beam has been discussed in great detail [11]. For simplicity, we assume that the partial neutralization is small and can be neglected here. As to the beams under investigation, the flow of particles can be considered laminar provided that

$$\frac{\nu}{\gamma} \equiv \frac{I}{I_A} \equiv \frac{I}{17000\ \beta\gamma} << 1$$

where Budker's parameter ν is the number of electrons per classical electron-radius length of the beam, γ is the relativistic factor of the beam particle, I is the beam current and I_A is the Alfven-Lawson limiting current [7]. The beam particles motion is taken to be paraxial ($P_z^2 >> P_r^2 + P_\theta^2$) where P_i denotes

the three components of the particle momentum in the i direction respectively. The axial velocity is very large compared to the transverse velocity and is considered to be a constant.

Analysis of dynamic properties is based on a macroscopic cold fluid model. The beams in equilibrium are assumed to be azimuthally symmetric ($\frac{\partial}{\partial \theta} = 0$), infinitely long and uniform axially ($\frac{\partial}{\partial z} = 0$). The equations of particle conservation and momentum conservation can be expressed in the relativistic form as

$$\frac{\partial n_i}{\partial t} + \nabla \cdot (n_i \underline{V}_i) = 0 \tag{1}$$

and

$$(\frac{\partial}{\partial t} + \underline{V}_i \cdot \nabla) \gamma_i m_i \underset{\sim}{V}_i = q_i (\underset{\sim}{E} + \underline{V}_i \times \underset{\sim}{B}) \tag{2}$$

where i = 1 or 2 denote the type of particles in the inner or outer beam respectively, q and m are the charge and rest mass of the particle, $n(x,t)$ and $\underset{\sim}{V}(x,t)$ are the density and mean velocity of the particle and $\underset{\sim}{E}(x,t)$ and $\underset{\sim}{B}(x,t)$ are the electric and magnetic fields respectively. The system with unknown variables such as n, $\underset{\sim}{V}$, $\underset{\sim}{E}$, $\underset{\sim}{B}$ can be closed by including the Maxwell's equations. The self-induced radial space-charge electric field and azimuthal magnetic field are calculated from Poisson's equation and Ampere's law which are shown below respectively

$$\nabla \cdot \underset{\sim}{E} = \varepsilon_0^{-1} q_i n_i \tag{3}$$

$$\nabla \times \underset{\sim}{B} = \mu_0 \, q_i \, V_{zi} \, n_i \, \hat{e}_z + \mu_0 \, \varepsilon_0 \, \frac{\partial \underset{\sim}{E}}{\partial t} \tag{4}$$

where μ_0 and ε_0 are permeability and permittivity of free space.

In the steady-state ($\frac{\partial}{\partial t} = 0$) the beam quantities are assumed axially and azimuthally symmetric ($\frac{\partial}{\partial z} = 0$ and $\frac{\partial}{\partial \theta} = 0$). Let us consider the following zero order equilibrium quantities

$$\underset{\sim}{V} = (0, V_\theta, V_Z)$$

$$\underset{\sim}{E} = (E_r, 0, 0)$$

$$\underset{\sim}{B} = (0, B_\theta, B_0)$$

From Eqs. (3) and (4), the fields inside the beams have the following form

$$E_r(r) = \begin{cases} q_1 \, n_1 \, (r^2 - R_1^2)/(2\varepsilon_0 r) & R_1 < r < R_2 \\ [q_1 n_1 (R_2^2 - R_1^2) + q_2 \, n_2 \, (r^2 - R_3^2)]/(2\varepsilon_0 r) & R_3 < r < R_4 \end{cases} \tag{5}$$

$$B_\theta(r) = \begin{cases} \mu_0 n_1 q_1 V_{z1} (r^2 - R_1^2)/2r & R_1 < r < R_2 \\ \mu_0 [q_1 n_1 V_{z1} (R_2^2 - R_1^2) + q_2 n_2 V_{z2} \, (r^2 - R_3^2)]/2r & R_3 < r < R_4 \end{cases} \tag{6}$$

In the zero order approximation, the balance between forces due to electric and magnetic field gives rise to the slow rotational equilibrium of the fluid element. One can readily obtain from Eq. (2) that there is only a radial component which supports the angular velocity $\omega_b(r)$ of the particle fluid element in slow rigid rotational equilibrium.

$$\omega_b(r) \equiv \frac{V_\theta}{r} = (V_z B_\theta - E_r)/rB_0 \tag{7}$$

where $\omega_c >> \omega_b$ has been assumed and $\omega_c \equiv qB_0/\gamma m$ is the angular cyclotron frequency. The radial dependence of B_θ and E_r has already been expressed in Eqs. (5) and (6). Note that the mean azimuthal motion of the beam particles is a function of r. Because of the angular rotation shear of the beam, the surface waves propagate relative to one another. Under suitable conditions, the interaction can become synchronized so as to produce a single exponentially growing transverse oscillation. Of course, the growth rate will be affected strongly by the beam parameters such as beam charge q, beam density n and beam velocity V_z . . . etc.

III. Stability analysis

We are seeking for the first-order perturbed quantities $\delta\hat{\Phi}$ such as δn, δV, δE and δB which are assumed to vary with θ, z and t according to

$$\delta\hat{\Phi}(x,t) = \delta\hat{\Phi}(r) \exp [j(\omega t - kz - \ell\theta)]$$

where the oscillating angular frequency ω is assumed to be complex with $\text{Im}\,\omega < 0$, k is the propagation wave number in the z direction and ℓ is the azimuthal harmonic number. Accordingly, we will use the following linear operators to linearize the set of Eqs. (1) thru (4)

$$\frac{\partial}{\partial t} \sim j\omega, \quad \frac{\partial}{\partial z} \sim - jk, \quad \frac{\partial}{\partial \theta} \sim - j\theta.$$

After some algebraic manipulation we obtain the following result for perturbed density

$$\delta n_i = \frac{\varepsilon_i(\delta\phi - V_{zi}\,\delta A_z)\,\ell}{rB_0\,(\omega - \ell\omega_b - kV_{zi})} \frac{\partial n}{\partial r} \qquad (8)$$

where ϕ and A are the scalar and vector potentials of the electromagnetic field with $\tilde{E} = - \nabla\phi$ and $\tilde{B} = \nabla \times \tilde{A}$. The sign of the charge, ± 1 is given by ε_i. With the help of the constants V_{z1} and V_{z2}, the perturbed fields $\delta\phi$ and δA_z can be linearly combined to form the following two coupling eigenvalue equations

$$\left(\frac{1}{r}\frac{\partial}{\partial r} r \frac{\partial}{\partial r} - \frac{\ell^2}{r^2}\right) \delta\psi_1 = - \varepsilon_0^{-1} [q_1 \delta n_1 (1 - \beta_1^2) + q_2\, \delta n_2 (1 - \beta_1\beta_2)] \qquad (9)$$

$$\left(\frac{1}{r}\frac{\partial}{\partial r} r \frac{\partial}{\partial r} - \frac{\ell^2}{r^2}\right) \delta\psi_2 = -\varepsilon_0^{-1}[q_1 \delta n_1 (1 - \beta_1\beta_2) + q_2\delta n_2(1 - \beta_2^2)] \qquad (10)$$

where $\delta\psi_1 \equiv \delta\phi - V_{z1}\,\delta A_z$ and $\delta\psi_2 = \delta\phi - V_{z2}\,\delta A_z$. Several assumptions have been made in deriving Eqs. (8), (9) and (10). Firstly, a tenuous particle beam with strong guiding magnetic field B_0 have been considered so that $\omega_c >> \omega_b$ or $\omega_c >> \omega_{pb}$ where ω_{pb} and ω_c are the beam particle plasma frequency and cyclotron frequency, respectively. Secondly the diocotron instability investigated here is characterized by a low frequency perturbation. Therefore, we consider only wavelengths long and frequencies low compared to quantities that characterize the beam radius R_b, i.e.,

$$|kR_b| << 1 \qquad \text{and} \qquad |\omega R_b| << \ell c$$

For the special case of a square constant density profile for each beam as illustrated in Figure 2, the contribution to the right-hand side of Eq. (8) becomes two delta functions at the sharp boundaries for each beam. The right-hand side of the eigenvalue Eqs. (9) and (10), are equal to zero except at the surface of the beam. Therefore the piece-wise solutions for the homogeneous Eqs. (9) and (10) can be expressed as

$$
\delta\psi_i(r) = \begin{cases}
\delta\psi_{i1}(r) = a_i r^{\ell} + b_i\, r^{-\ell} & 0 < r < R_1 \\
\delta\psi_{i2}(r) = c_i r^{\ell} + d_i\, r^{-\ell} & R_1 < r < R_2 \\
\delta\psi_{i3}(r) = e_i\, r^{\ell} + f_i\, r^{-\ell} & R_2 < r < R_3 \\
\delta\psi_{i4}(r) = g_i\, r^{\ell} + h_i\, r^{-\ell} & R_3 < r < R_4 \\
\delta\psi_{i5}(r) = i_i\, r^{\ell} + j_i\, r^{-\ell} & R_4 < r < R_c
\end{cases} \qquad (11)
$$

where the solutions with i = 1 or 2 are corresponding to Eqs. (9) or (10) respectively. The coefficients a_i, b_i... are functions of R_1, R_2 ... R_c to be determined by the boundary conditions, the requirement imposed by delta functions. In other words the eigenfunction is continuous at each boundary and vanishes both at r = 0 and r = R_c. In addition, the contribution from four delta functions can be obtained by integrating the eigenvalue equation across the discontinuities. Following the same procedure as one does in [4], we obtain totally 20 relationships which are listed below for reference. First we obtain from Eq. (1) the following 10 conditions

$$\delta\psi_{11}(0) = 0$$

$$\delta\psi_{11}(R_1) = \delta\psi_{12}(R_1)$$

$$\delta\psi'_{12}(R_1) - \delta\psi'_{11}(R_1) = \frac{2\ell\ \varepsilon_1\ \delta\psi_{11}(R_1)}{N\,(X - Y_0)\,R_1}$$

$$\delta\psi_{12}(R_2) = \delta\psi_{13}(R_2) \qquad (12)$$

$$\delta\psi'_{13}(R_2) - \delta\psi'_{12}(R_2) = -\frac{2\ell\ \varepsilon_1\ \delta\psi_{12}(R_2)}{N\,(X - Y_1)\,R_2}$$

$$\delta\psi_{13}(R_3) = \delta\psi_{14}(R_3)$$

$$\delta\psi'_{14}(R_3) - \delta\psi'_{13}(R_3) = -\frac{2\ell\ \delta\psi_{13}(R_3)\ X_2}{(X - Y_2)\ R_3}$$

$$\delta\psi_{14}(R_4) = \delta\psi_{15}(R_4)$$

$$\delta\psi'_{15}(R_4) - \delta\psi'_{14}(R_4) = \frac{2\ell\ \delta\psi_{14}(R_4)\ X_2}{(X - Y_3)\ R_4} \qquad (12)$$

$$\delta\psi_{15}(R_c) = 0$$

Similary, we obtain from Eq. (10) the following 10 relationships

$$\delta\psi_{21}(0) = 0$$

$$\delta\psi_{21}(R_1) = \delta\psi_{22}(R_1)$$

$$\delta\psi'_{22}(R_1) - \delta\psi'_{21}(R_1) = \frac{2\ell\ \varepsilon_1\ \delta\psi_{21}(R_1)\ X_1}{N\ (X - Y_0)\ R_1}$$

$$\delta\psi_{22}(R_2) = \delta\psi_{23}(R_2)$$

$$\delta\psi'_{23}(R_2) - \delta\psi'_{22}(R_2) = -\frac{2\ell\ \varepsilon_1\ \delta\psi_{22}(R_2)\ X_1}{N\ (X - Y_1)\ R_2} \qquad (13)$$

$$\delta\psi_{23}(R_3) = \delta\psi_{24}(R_3)$$

$$\delta\psi'_{24}(R_3) - \delta\psi'_{23}(R_3) = -\frac{2\ell\ \delta\psi_{23}(R_3)}{(X - Y_2)\ R_3}$$

$$\delta\psi_{24}(R_4) = \delta\psi_{25}(R_4)$$

$$\delta\psi'_{25}(R_4) - \delta\psi'_{24}(R_4) = \frac{2\ell\ \delta\psi_{24}(R_4)}{(X - Y_3)\ R_4} \qquad (13)$$

$$\delta\psi_{25}(R_c) = 0$$

where the prime denotes differentiation with respect to r and the following abbreviations have been used:

$$X = \frac{\omega}{\omega_D}$$

$$Y_0 = \frac{kV_{z1}}{\omega_D}$$

$$Y_1 = \frac{kV_{z1}}{\omega_D} - \varepsilon_1 \ell\ (R_2^2 - R_1^2) / (NR_2^2)$$

$$Y_2 = \frac{kV_{z2}}{\omega_D} - \varepsilon_1\ \ell\ X_1\ (R_2^2 - R_1^2) / (NR_3^2)$$

$$Y_3 = \frac{kV_{z2}}{\omega_D} - \varepsilon_1\ \ell\ X_1\ (R_2^2 - R_1^2) / (NR_4^2) + \ell\ (R_4^2 - R_3^2) / R_4^2$$

$$N = \frac{\omega_{D2}}{\omega_{D1}}$$

$$X_1 = \gamma_1^2\ (1 - \beta_1\beta_2)$$

$$X_2 = \gamma_2^2\ (1 - \beta_1\beta_2)$$

$$\omega_D = \omega_{D2}$$

The diocotron frequencies ω_{Di} are defined by $\omega_{Di} \equiv \omega_{pbi}^2 / 2\gamma_i^2\ \omega_{ci}$ where i = 1 for inner beam and i = 2 for outer beam. Therefore we have the dispersion

relation given by 20 equations with 20 unknowns. For a solution to exist, the determinant of the homogeneous linear set of equations must be equal to zero. In practice, a straight forward algebraic manipulation leads us to the following important relationships.

$$d_2 = d_1 X_1$$

$$f_2 = f_1 X_1 \tag{14}$$

$$e_2 = [e_1 R_c^{2\ell} + f_1 (1 - X_1 X_2)] / R_c^{2\ell} X_2$$

Under the circumstance of $\beta_1 = \beta_2$, we can obtain easily that $d_2 = d_1$, $f_2 = f_1$ and $e_2 = e_1$. The two eigenvalues, Eqs. (9) and (10), become essentially identical. It goes back exactly to the case of coaxial multi-ring electron beam we have studied before [4]. For the general case, Eqs. (12) and (13) have to be solved simultaneously. After some elementary but tedious algebra, we obtain finally the following dispersion relation which is a quartic polynomial equation

$$x^4 + c_1 x^3 + c_2 x^2 + c_3 x + c_4 = 0 \tag{15}$$

IV. Numerical results

The dispersion relation (15) is solved numerically to determine the growth rate and oscillating frequency of the instability as a function of wavenumber k in terms of various beam parameters and geometries. We are primarily interested in the perturbations with lower azimuthal mode numbers ℓ, especially the mode with $\ell = 1$ which corresponds to a sideways displacement of the whole beam. This is the most dangerous kink mode perturbation which causes the asymmetry of the beam and triggles the break up of the beam. In principle, the same mechanism that accelerates electrons can also accelerate ions. Therefore it is more appropriate to include both situations in the following stability analysis.

First, we will consider the electron accelerator. In this case both beam particles are singly charged electrons. It can be described more specifically in the following cases

$$\text{(a)} \quad q_1 = q_2 = -e, \ \beta_1 = |\beta_1| \hat{e}_z, \ \beta_2 = -|\beta_2| \hat{e}_z.$$

Two electron beams propagate in the opposite axial direction with velocities β_1 and β_2 respectively. It turns out to be the most unstable configuration in the system when both beams have the same energy, i.e., $|\beta_1| = |\beta_2|$. The growth rate and real frequency of the instability are shown in Figure 3 versus wavenumber for the modes with ℓ =1 and 2. In order to illustrate the effect of geometry and density of two beams on instability, three different beam locations are chosen with two different values of n_1/n_2, the number density ratio of inner beam n_1 to outer beam n_2. For convenience, we fix the location of the outer annular electron beam between radius r_3 = .85

R_c and $R_4 = .95\ R_c$ and place the inner electron beam with the same thickness ($R_2 - R_1 = R_4 - R_3$) at three different locations. First, when $r_1 = R_3$ the inner beam coincides with the outer beam, the growth rate for $\ell = 2$ is larger than $\ell = 1$ and both have the magnitude of several times of $\omega_D \equiv \omega_{D2}$, the diocotron frequency of the outer electron beam. As r_1 decreases half-way ($r_1 = R_3/2$) the growth rates for $\ell = 1$ and 2 decreases and become comparable to each other. Finally, when $r_1 = 0$, i.e., the inner beam becomes essentially a solid beam, the growth rates decrease further with $\ell = 1$ mode dominates the instability which agrees with those obtained by Uhm [8]. Note that in these calculations the inner beam with the same thickness and density numbers at three different locations carry three different amounts of current. Another important feature of Figure 3 is that the growth rates increase as the ratio of n_1/n_2 increases. More specifically, the growth rate varies directly proportional to $\sqrt{n_1/n_2}$. If there is a requirement for the inner beam to carry the same current at three different locations as indicated in Figure 3, the growth rate in three cases are all comparable. It is concluded that the counter two-stream electron beams is the most unstable set up and therefore has to be avoided in the accelerator experiment. Otherwise, the inner beam has not only to carry less current but also to be as thin as possible and keep distance from the outer beam. Because the fluid element of each beam rotates around the axis in the opposite direction, the self-induced fields therefore oppose to each other and have the tendency to break the equilibrium configuration easily. As far as the wave mode competition, it seems that the kink mode ($\ell = 1$) is more unstable when there is an inner solid beam. Finally and most importantly, in Figure 3 the real frequency ω_R for the oscillation is nearly a constant versus wavenumber k.

So that the group velocity is very small compared to c, i.e., $0 \leq V_g < c$. It is a critical criteria while considering the finite geometry effect which will be discussed later.

(b) $q_1 = q_2 = -e$, $\underset{\sim}{\beta}_1 = \underset{\sim}{\beta}_2$.

In this case the two electron beams may actually come from the same source in the laboratory. The diocotron instability of the coaxial multi-ring hollow electron beam has been studied extensively before [4]. For the purpose of comparison, we do the similar calculations as those in Figure 3 except that $\underset{\sim}{\beta}_1 = |\beta_2| \hat{e}_z$. The results are shown in Figure 4 with a few distinctions. As we can see immediately, the $\ell = 1$ mode is stable all the time as indicated in the previous paper [4]. The growth rates for $\ell = 2$ are relatively small and no longer a function of wavenumber. However, in contrast with those in Figure 3 the group velocity can be very large. It seems that the group velocity can be very large whenever the growth rate is small and vise versa. Generally speaking, the growth rate dereases when the gap between two beams increases. For the same beam geometry, the increase of n_1/n_2 will enhance the growth rate.

(c) $q_1 = q_2 = -e$, $-\underset{\sim}{\beta}_2 < \underset{\sim}{\beta}_1 < \underset{\sim}{\beta}_2$.

In most of the collective particle accelerators, the beam particles, whether they are propagating at the same direction or opposite to each other, do not have to travel at the same speed. In light of this, we add another figure here to demonstrate the evolution of growth rates due to the change of $\underset{\sim}{\beta}_1$ from, $-|\beta_2| \hat{e}_z$ to $|\beta_2| \hat{e}_z$. Namely, we do the same exercises as those in

Figure 3 or Figure 4 except that $\underset{\sim}{\beta}_1 = 0$. The results are shown in Figure 5 which gives an intermediate picture between Figure 3 and Figure 4. As one can see clearly that the growth rates in most cases are moderate even for $\beta_1 = 0$. In other words, the electron plasma have an important effect on the diocotron instability of a hollow electron beam [9], [10]. At this stage, it is apparent that the counter two electron beams will suffer the most as far as the transverse oscillation is concerned. Finally, in most collective electron accelerators, the inner beam is solid, i.e. $R_1 = 0$. We demonstrate in Figure 6 as a final example the growth rate of the instability for a solid electron beam with various velocities propagating through an annular electron beam. As $\underset{\sim}{\beta}_1$ change gradually from $-|\beta_2|$ to $|\beta_2|$, the growth rates for $\ell = 1$ and 2 modes decrease. There is no doubt that it is more stable to have two electron beams propagate in the same direction.

Next, as we turn our attention to the collective ion accelerator, we consider the case where $q_1 = +e$, $q_2 = -e$ and $R_1 = 0$, i.e., the inner beam particle is a solid beam and carries singly charged ion. In collective ion accelerators, a high-power relativistic electron beam is used to accelerate a beam of positive ions to high energy. This process is achieved through the use of the collective fields of the primary electron beam. The effect of ion background on diocotron instability of an annular electron beam has been studied in connection with autoaccelerator [11]. Nevertheless, we have extended here the perturbation to the axial direction with finite wavenumber k. Recall that in our theory of perturbation, the condition of $\omega_{pbi} << \omega_{ci}$ was used in deriving Eqs. (8), (9) and (10), where ω_{pb} and ω_c are the plasma and cyclotron frequency of the beam particle species electron or ion. Because of the large mass of the ion comparing to the electron (e.g., $m_i = 1840\ m_e$), it

might be difficult to find the experimental condition with beam parameters satisfying the requirement of $\omega_{pbi} << \omega_{ci}$. If the condition $\omega_{pbi} << \omega_{ci}$ fails or even $\omega_{pbi} \simeq \omega_{ci}$, the theory of perturbation derived in Section III is no longer valid. The additional terms have to be kept in the dispersion relation (e.g., Eq. (2.6.20) of [12] or Eq. (6) of [13]). The theory of perturbation for this particular beam parameter is currently under investigation. However, as long as the requirement of $\omega_{pbi} << \omega_{ci}$ is fulfilled then the formalism is still valid. We choose a few examples to demonstrate the results.

In Figure 7 the growth rates have been shown versus wavenumber for $\beta_1 = -.1$, 0 and .1 respectively. When $\gamma_2 = 10$ and $n_1/n_2 = .01$, the growth rates are relatively small and become almost a constant for larger $|k|$. The magnitude of β_1 is so small that the effect of ion speed on instability is virtually unseen. This is what we should expect from the conventional diocotron instability under the influence of the ion background. If we reduce γ_2 from 10 to 4 and change β_1 from -.2 to .2 instead of from -.1 to .1. The growth rates decreases and become almost independent of wavenumber k as illustrated in Figure 8. Note that in Figures 7 and 8, the $\ell = 1$ is always unstable as predicted in [11] due to the influence of the background ions. In the particle simulation for a long pulse accelerator, the ions created from the wall will travel towards the center of the tube. Because of the formation of the virtual anode near the center, the ions do not go through or move very close to the center of the tube. Instead they are reflected and travel back towards the wall. It is likely that we can have two sets of ion distribution, e.g., one from r = 0 to .8 R_c, and the other from

$r = .2\ R_c$ to R_c. The growth rates versus wavenumber are shown in Figure 9 for three different values of n_1/n_2. The increase of the ion number density clearly will enhance the instability which has been observed before [11].

V. Discussions

The stability analysis for the case of infinitely long coaxial multiple beams has been studied using the fluid-Maxwell model. The stability property has been illustrated in great detail for a variety of experimentally interesting circumstances. In summary, for the electron-electron transverse oscillation it is more unstable when the two electron beams move in the opposite direction. Because the most dangerous kink mode can be destabilized with growth rate a few times of the diocotron frequency. It is similar to the resonant counter two-stream instability. On the other hand, if the beams travel in the same direction, the kink mode becomes stable and the growth rate for $\ell = 2$ mode is only a few tenths of diocotron frequency. It is essentially a conventional diocotron instability. As to the ion-electron transverse oscillation, two beam particles can not interact each other closely in the parameter regime where the plasma frequency is much smaller than the cyclotron frequency for both ions and electrons. Therefore, the resonant two-stream instability is not observed. In the light of the collective particle accelerator, supressing the transverse oscillation or reducing the growth rate to a tolerable level is a necessary requirement for a successful accelerator. Although some of the features in the real device such as the beam density modulation and spatial variation of the magnetic field have been left out in the calculations. As a reminder, we want to mention that the growth rates calculated in Section IV have been normalized to the diocotron frequency ω_D of the outer annular beam. From the definition of the diocotron frequency ω_D which is a function of static magnetic field B_0 and relativistic scaling factor γ. The growth rate can be easily reduced by either increasing

the kinetic energy of the annular beam or increasing the applied magnetic field. Other methods of reducing the growth rate can also be found by adjusting the beam geometry and parameters.

In the real device of the collective particle accelerator, most importantly the effect of finite geometry on the transverse oscillation, has to be taken into account. For any convective instability, knowing the growth rate is not quite enough, we have to know the group velocity to show how fast the waves propagate. As to the collective electron accelerator, it has been concluded that the growth rate can be very large because of the counter two-stream instability. However, if one looks carefully from Figure 3 and Figure 5, the real frequency of oscillation is almost a constant while varying the wave number k. Therefore, the group velocity V_g is very small compared to the beam velocity V, i.e., $0 \leq V_g << V \simeq c$. One finds from the wave kinetic equation that the peak of the wave is very far away from reaching the beam head. In this sense, one can almost be certain that the instability does not prevent acceleration of the beam head in the experiment. Another idea of chopping the electron beam will undoubtly prevent the instability from continuing to grow and follow the beam head.

In the collective ion accelerator, the numerical result has indicated that the group velocity is very large compared to the slow ion beam velocity V, i.e., $V_g > V$. This means that the transverse oscillation has the maximum at the head of the beam. Fortunately, the growth rates for the ion-electron transverse oscillations are relatively small. Furthermore, the growth rate can be reduced very much by simply reducing the radius of the ion beam.

ACKNOWLEDGEMENTS

This research was supported in part by the Independent Research Fund at the Naval Surface Weapons Center and in part by the Office of Naval Research.

REFERENCES

1. M. Friedman, IEEE Trans. Nucl. Sci., Vol. NS-26, p. 4186, 1979.

2. T. R. Lockner and M. Friedman, IEEE Trans. Nucl. Sci., Vol. NS-26, p. 4237, 1979.

3. M. Friedman, "A new collective particle accelerator," NRL Mem. Rep. 3724, Feb. 1978.

4. H. C. Chen and P. J. Palmadesso, Phys. Fluids, Vol. 24, p. 357, 1981.

5. H. S. Uhm and J. G. Siambis, Phys. Fluids, Vol. 22, p. 2377, 1979.

6. W. W. Destler, H. S. Uhm, H. Kim and M. P. Reiser, J. Appl. Phys., Vol. 50, p. 3015, 1979.

7. J. D. Lawson, The Physics of Charged-Particle Beams, Clarendon Press, Oxford, 1977, Ch. 3.

8. H. S. Uhm, Phys. Fluids, Vol. 25, p. 1908, 1982.

9. D. A. Whelan and R. L. Stenzel, Phys. Rev. Lett., Vol. 47, p. 95, 1981.

10. H. S. Uhm and R. C. Davidson, Phys. Fluids, Vol. 23, p. 813, 1980.

11. H. C. Chen (to be published in J. Appl. Phys.)

12. R. C. Davidson, Theory of Non-Neutral Plasmas, Benjamin, New York, 1974, Ch. 2.

13. H. C. Chen and H. S. Uhm, IEEE Trans. Nucl. Sci., Vol. NS-30, p. 2004, 1983.

FIGURE CAPTIONS

Figure 1 — Longitudinal and cross section of equilibrium configuration and coordinate system.

Figure 2 — Beam particle density for two-beam geometry.

Figure 3 — Growth rate $\frac{\omega_i}{\omega_D}$ and real frequency $\frac{\omega_R}{\omega_D}$ of the electron-electron transverse oscillation (ℓ = 1 and 2) VS wavenumber $\frac{kc}{\omega_D}$ for various R_1 and $\frac{n_1}{n_2}$ when $R_3 = .85\ R_c$, $R_4 = .95\ R_c$, $R_4 - R_3 = R_2 - R_1$, $\beta_1 = -\beta_2$ and $\gamma = 4$.

Figure 4 — Similar to Figure 3, except $\beta_1 = \beta_2$.

Figure 5 — Similar to Figure 3 except $\gamma_1 = 1$ and $\gamma_2 = 4$.

Figure 6 — Growth rate $\frac{\omega_i}{\omega_D}$ of the electron-electron transverse oscillation (ℓ = 1 and 2) VS wavenumber $\frac{kc}{\omega_D}$ for various β_1 when $\gamma_2 = 4$, $R_1 : R_2 : R_3 : R_4 = 0 : .2 : .857 : .939$ and $n_1 = n_2$.

Figure 7 — Growth rate $\frac{\omega_i}{\omega_D}$ and real frequency $(\omega_R - kV_1)/\omega_D$ of the electron-ion transverse oscillation (ℓ = 1 and 2) VS wavenumber $\frac{kc}{\omega_D}$ for various β_1 when $\gamma_2 = 10$, $\frac{n_1}{n_2} = .01$ and $R_1 : R_2 : R_3 : R_4 = 0 : .8 : .837 : .939$.

Figure 8 — Similar to Figure 7 except for various β_1 and $\gamma_2 = 4$.

Figure 9 The affect of ion background on the diocotron instability of an annular electron beam.

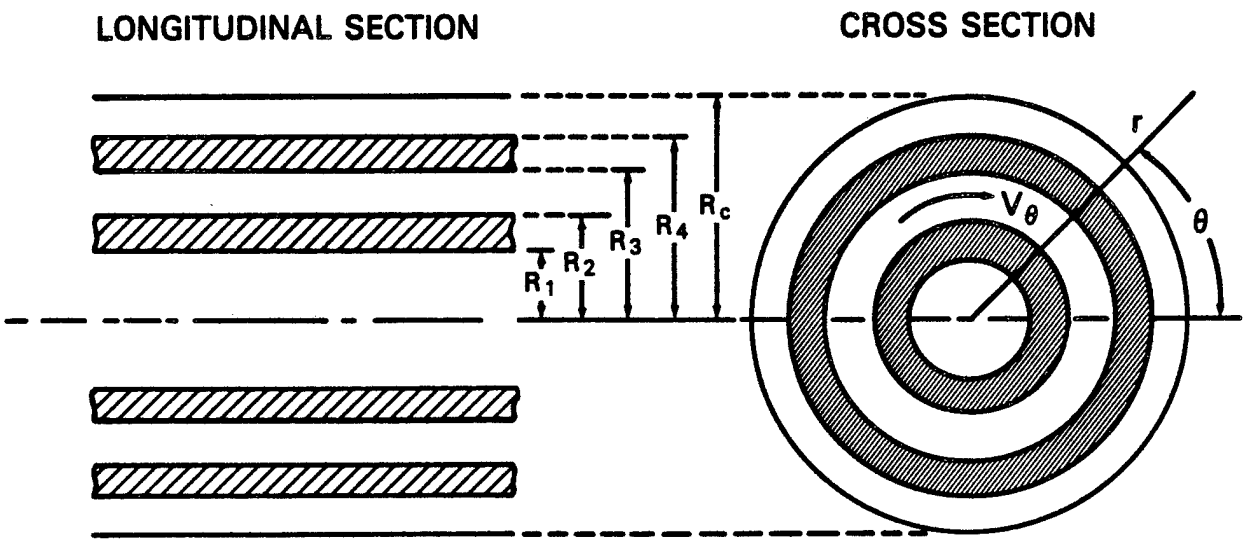
LONGITUDINAL SECTION
CROSS SECTION
R_1
R_2
R_3
R_4
R_c
r
V_θ
θ

Figure 1

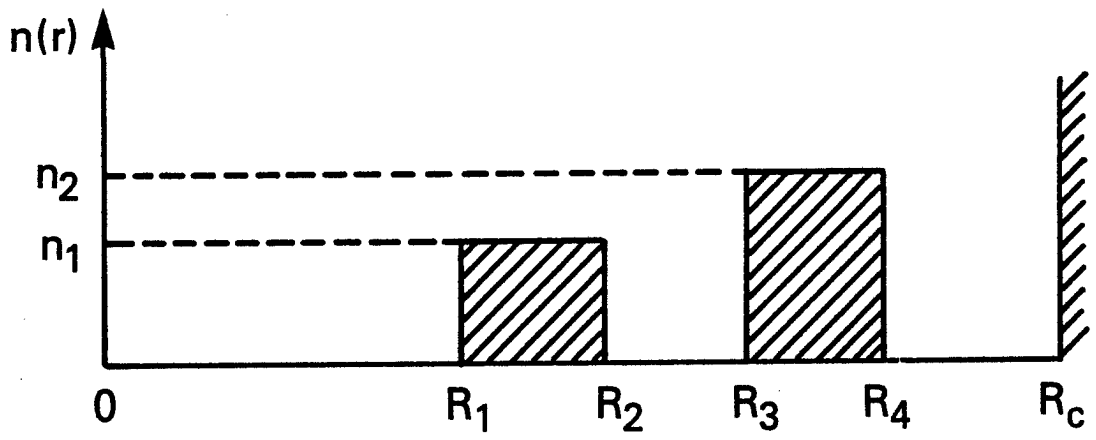

Figure 2

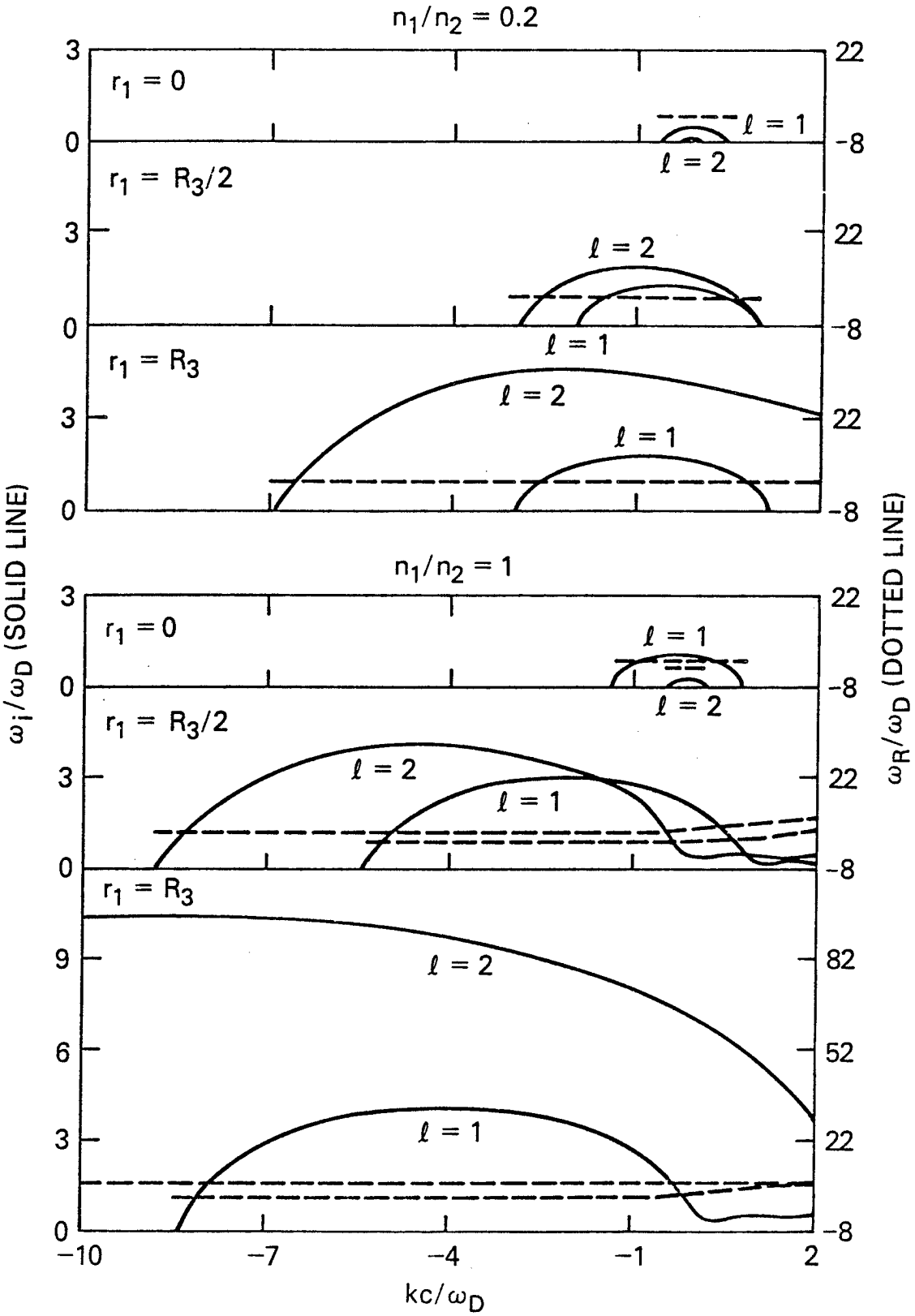
$n_1/n_2 = 0.2$
$r_1 = 0$
$r_1 = R_3/2$
$r_1 = R_3$
$\ell = 1$
$\ell = 2$
$n_1/n_2 = 1$
ω_i/ω_D (SOLID LINE)
ω_R/ω_D (DOTTED LINE)
kc/ω_D
3
0
9
6
22
-8
82
52
-10
-7
-4
-1
2

Figure 3

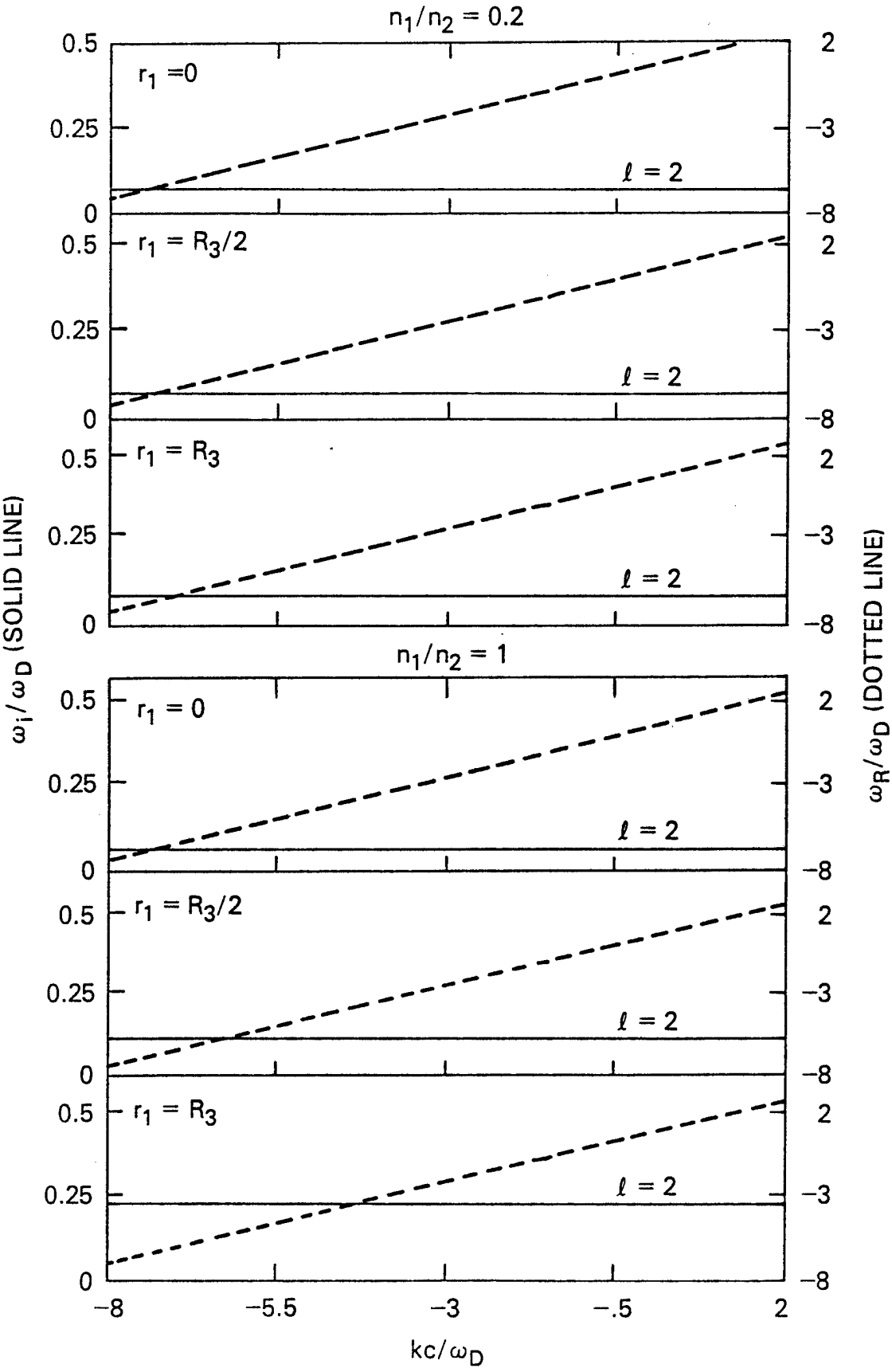
$n_1/n_2 = 0.2$
$r_1 = 0$
$r_1 = R_3/2$
$r_1 = R_3$
$n_1/n_2 = 1$
$r_1 = 0$
$r_1 = R_3/2$
$r_1 = R_3$
$\ell = 2$
0.5
0.25
0
2
−3
−8
−8
−5.5
−3
−.5
2
ω_i/ω_D (SOLID LINE)
ω_R/ω_D (DOTTED LINE)
kc/ω_D

Figure 4

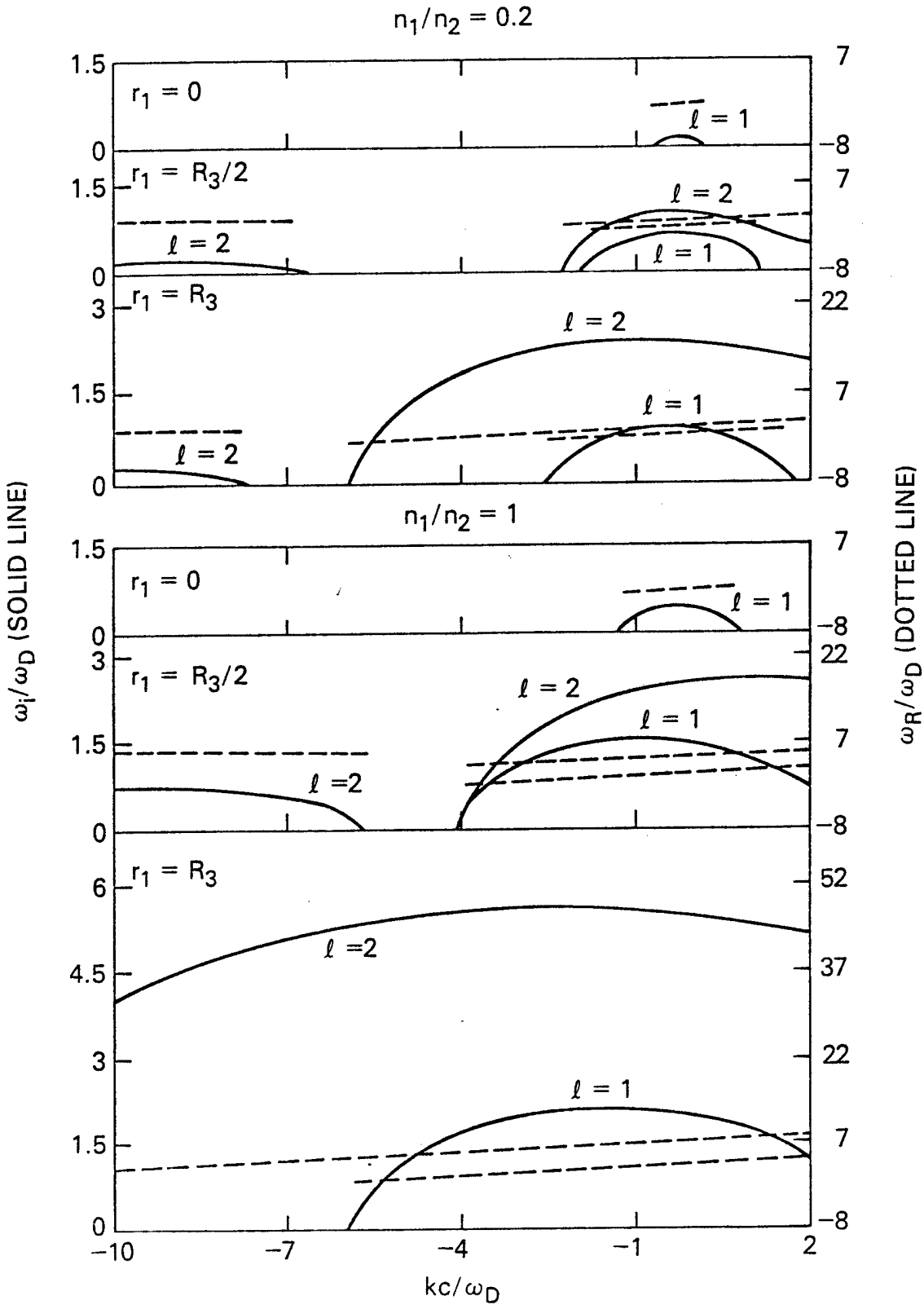
$n_1/n_2 = 0.2$
$r_1 = 0$
$\ell = 1$
$r_1 = R_3/2$
$\ell = 2$
$\ell = 2$
$\ell = 1$
$r_1 = R_3$
$\ell = 2$
$\ell = 1$
$\ell = 2$
$n_1/n_2 = 1$
$r_1 = 0$
$\ell = 1$
$r_1 = R_3/2$
$\ell = 2$
$\ell = 1$
$\ell = 2$
$r_1 = R_3$
$\ell = 2$
$\ell = 1$
1.5
0
3
6
4.5
7
−8
22
52
37
−10
−7
−4
−1
2
kc/ω_D
ω_i/ω_D (SOLID LINE)
ω_R/ω_D (DOTTED LINE)

Figure 5

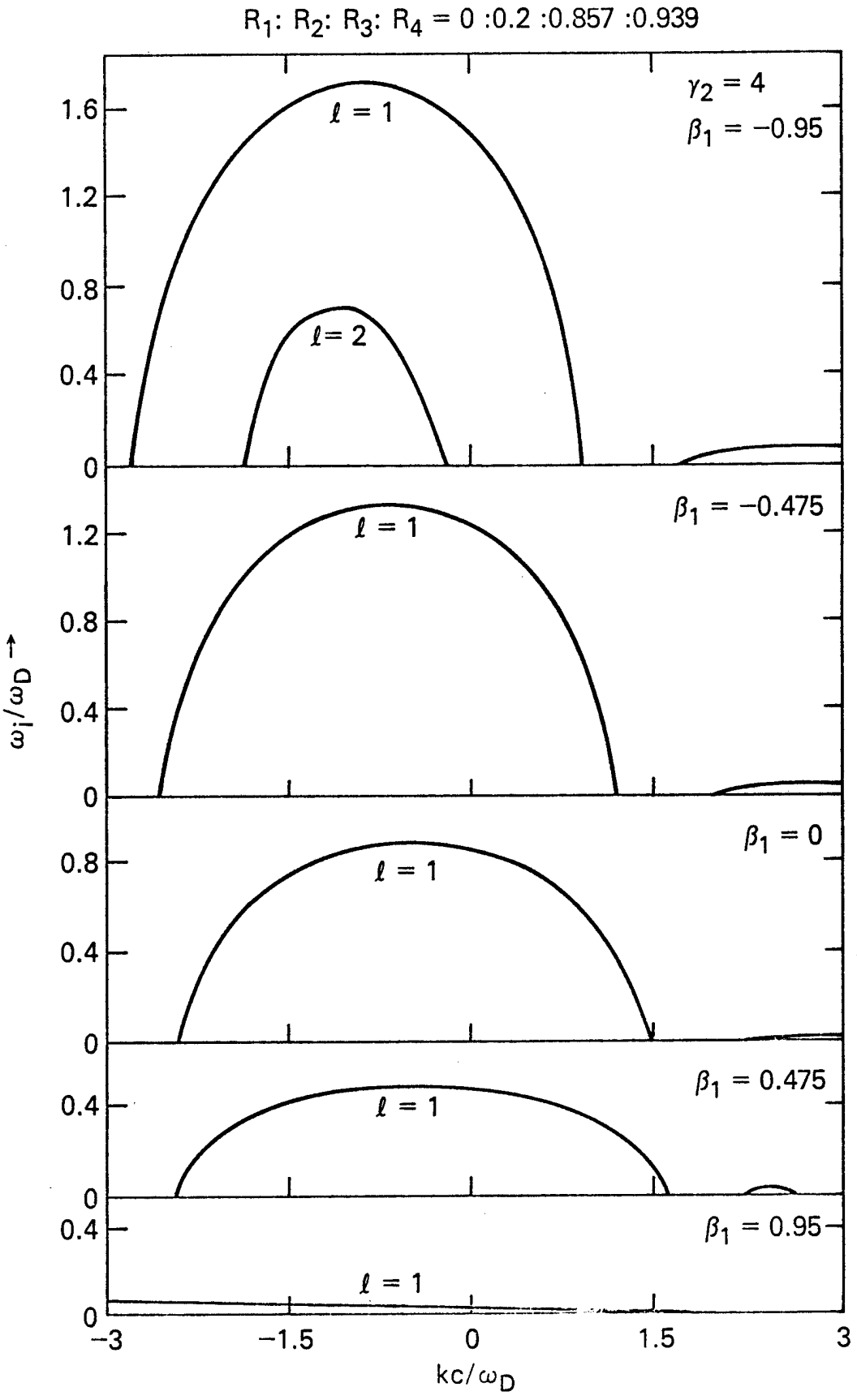
R_1: R_2: R_3: R_4 = 0 :0.2 :0.857 :0.939
$\gamma_2 = 4$
$\beta_1 = -0.95$
$\ell = 1$
$\ell = 2$
$\beta_1 = -0.475$
$\ell = 1$
$\beta_1 = 0$
$\ell = 1$
$\beta_1 = 0.475$
$\ell = 1$
$\beta_1 = 0.95$
$\ell = 1$
ω_i/ω_D
kc/ω_D
1.6
1.2
0.8
0.4
0
−3
−1.5
1.5
3

Figure 6

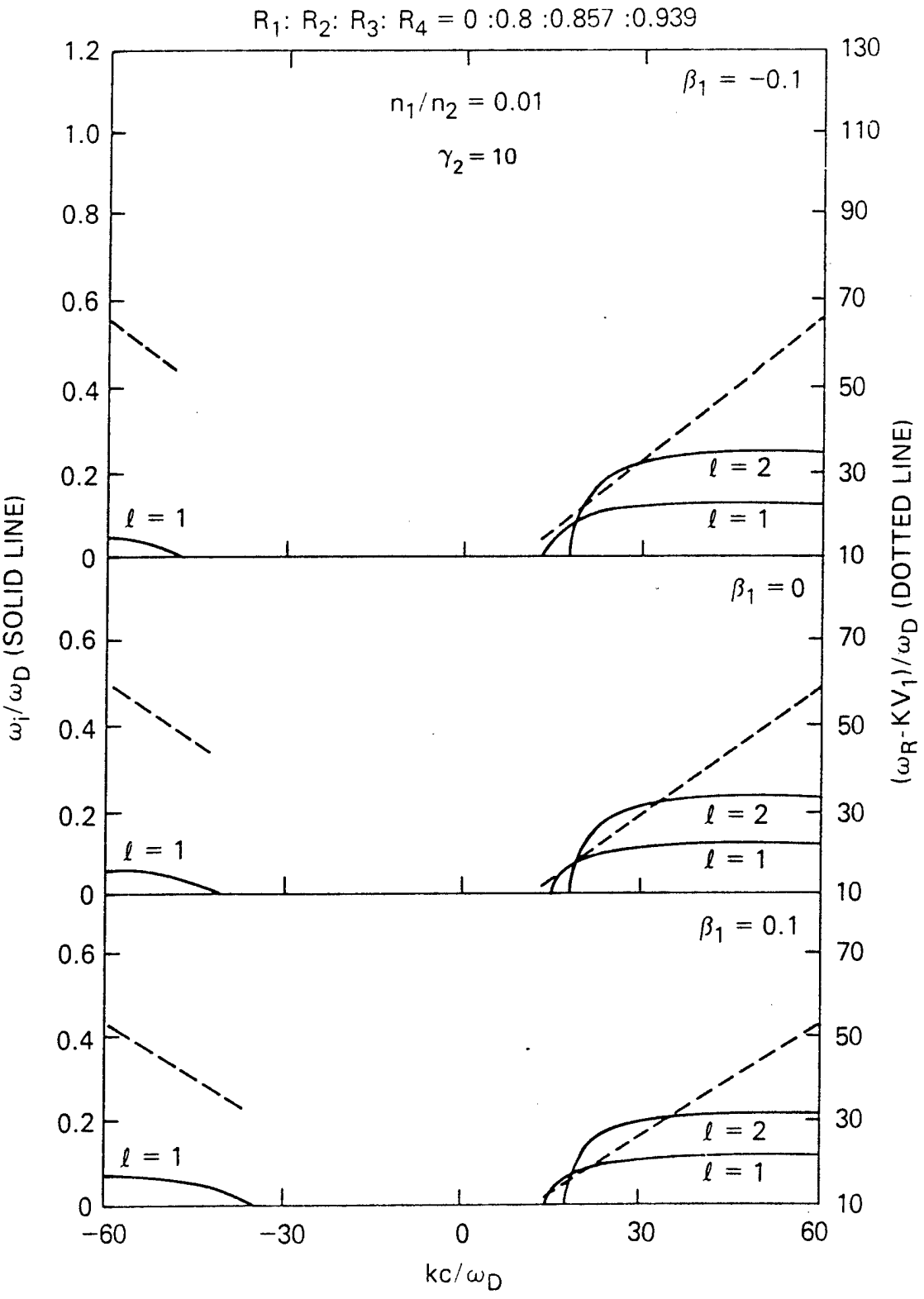
R_1: R_2: R_3: R_4 = 0 :0.8 :0.857 :0.939
$\beta_1 = -0.1$
$n_1/n_2 = 0.01$
$\gamma_2 = 10$
$\beta_1 = 0$
$\beta_1 = 0.1$
$\ell = 1$
$\ell = 2$
ω_i/ω_D (SOLID LINE)
$(\omega_R - KV_1)/\omega_D$ (DOTTED LINE)
kc/ω_D
1.2
1.0
0.8
0.6
0.4
0.2
0
130
110
90
70
50
30
10
−60
−30
0
30
60

Figure 7

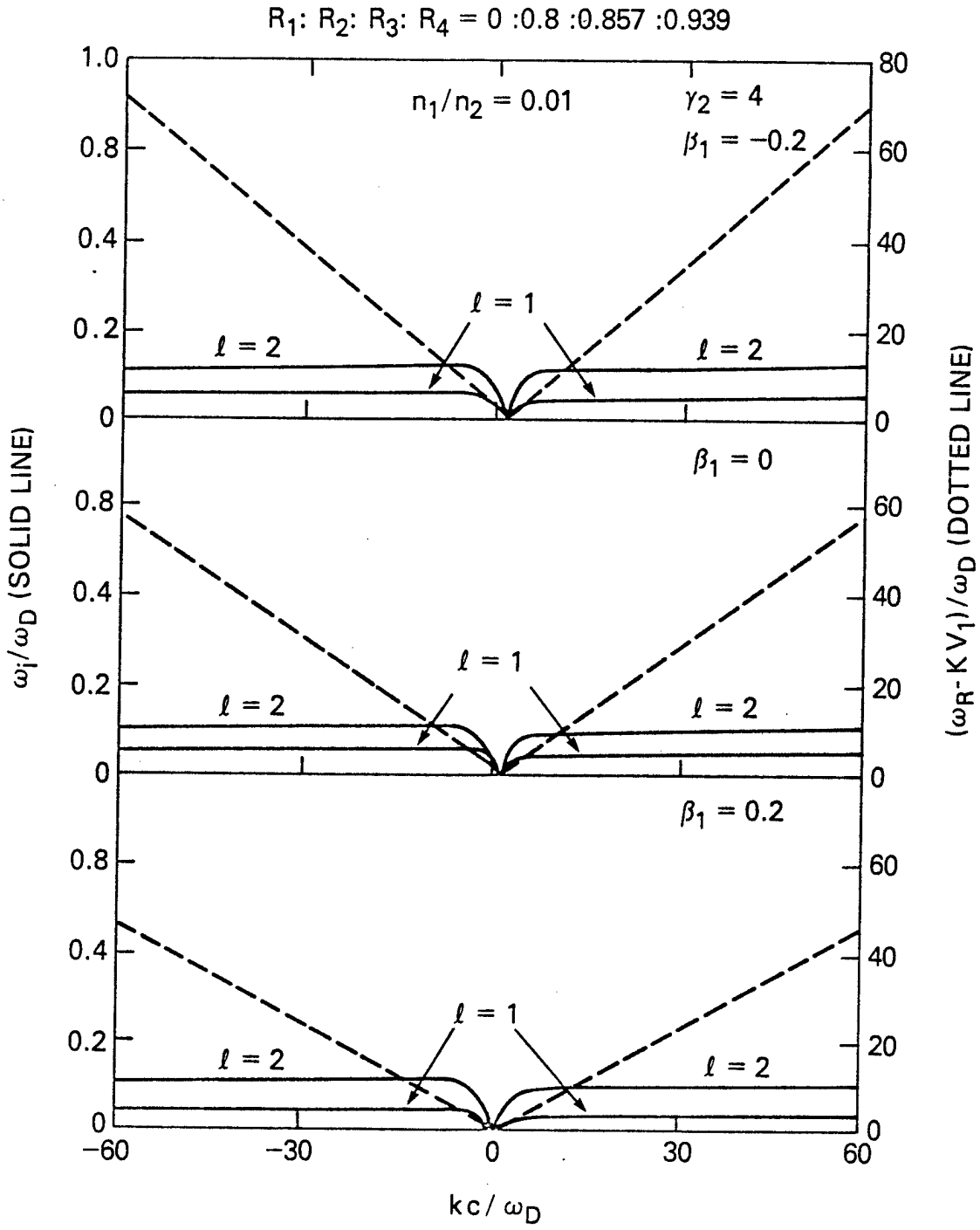
R_1: R_2: R_3: R_4 = 0 :0.8 :0.857 :0.939
n_1/n_2 = 0.01
γ_2 = 4
β_1 = −0.2
β_1 = 0
β_1 = 0.2
ℓ = 1
ℓ = 2
ω_i/ω_D (SOLID LINE)
$(\omega_R - KV_1)/\omega_D$ (DOTTED LINE)
kc/ω_D
1.0
0.8
0.4
0.2
0
80
60
40
20
−60
−30
30
60

Figure 8

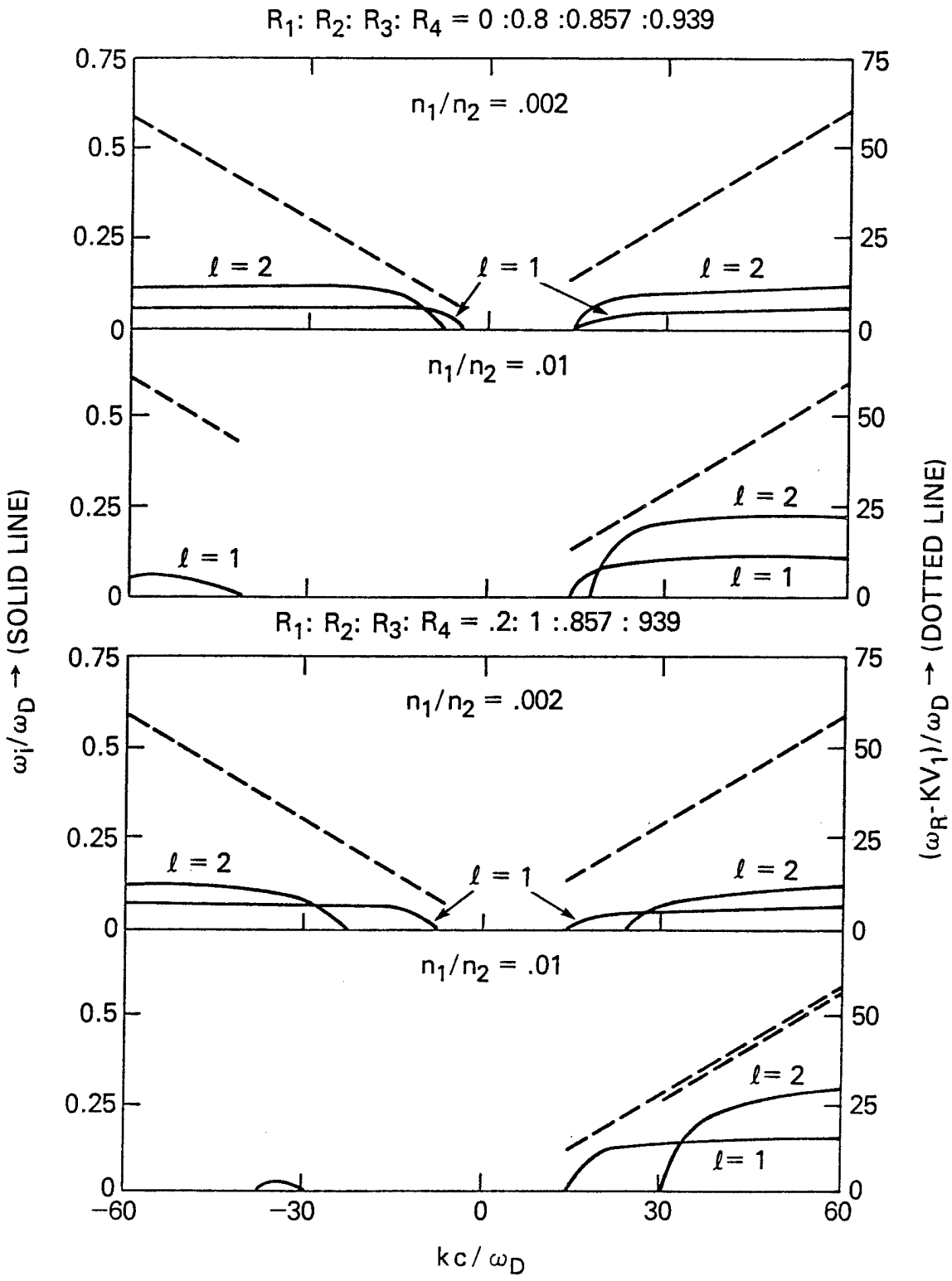
R1: R2: R3: R4 = 0 :0.8 :0.857 :0.939
n1/n2 = .002
n1/n2 = .01
ℓ = 2
ℓ = 1
R1: R2: R3: R4 = .2: 1 :.857 : 939
n1/n2 = .002
n1/n2 = .01
ℓ = 2
ℓ = 1
0.75
0.5
0.25
0
75
50
25
0
−60
−30
0
30
60
kc/ωD
ωi/ωD → (SOLID LINE)
(ωR-KV1)/ωD → (DOTTED LINE)

Figure 9